
















# Terahertz quantum cascade laser under optical feedback: effects of laser self-pulsations on self-mixing signals

XIAOQIONG QI,<sup>1</sup>  KARL BERTLING,<sup>1</sup>  THOMAS TAIMRE,<sup>2</sup>  GARY AGNEW,<sup>1</sup>  YAH LENG LIM,<sup>1</sup>  TIM GILLESPIE,<sup>1</sup>  ALEKSANDAR DEMIĆ,<sup>3</sup>  PAUL DEAN,<sup>3</sup>  LIAN HE LI,<sup>3</sup>  EDMUND H. LINFIELD,<sup>3</sup>  A. GILES DAVIES,<sup>3</sup>  DRAGAN INDJIN,<sup>3</sup>  AND ALEKSANDAR D. RAKIĆ<sup>1,\*</sup> 

<sup>1</sup>*School of Information Technology and Electrical Engineering, The University of Queensland, Brisbane, QLD 4072, Australia*

<sup>2</sup>*School of Mathematics and Physics, The University of Queensland, Brisbane, QLD 4072, Australia*

<sup>3</sup>*School of Electronic and Electrical Engineering, University of Leeds, Leeds LS2 9JT, UK*

\*[rakic@itee.uq.edu.au](mailto:rakic@itee.uq.edu.au)

**Abstract:** In this article, we explore the interplay between the self-pulsations (SPs) and self-mixing (SM) signals generated in terahertz (THz) quantum cascade lasers (QCLs) under optical feedback. We find that optical feedback dynamics in a THz QCL, namely, SPs, modulate the conventional SM interference fringes in a laser feedback interferometry system. The phenomenon of fringe loss in the SM signal — well known in interband diode lasers — was also observed along with pronounced SPs. With an increasing optical feedback strength, SM interference fringes transition from regular fringes at weak feedback ( $C \leq 1$ ) to fringes modulated by SPs under moderate feedback ( $1 < C \leq 4.6$ ), and then [under strong feedback ( $C > 4.6$ )] to a SM waveform with reduced number of fringes modulated by SP, until eventually (under even greater feedback) all the fringes are lost and only SPs are left visible. The transition route described above was identified in simulation when the SM fringes are created either by a moving target or a current modulation of the THz QCL. This SM signal transition route was successfully validated experimentally in a pulsed mode THz QCL with SM fringes created by current modulation during the pulse. The effects of SP dynamics in laser feedback interferometric system investigated in this work not only provides a further understanding of nonlinear dynamics in a THz QCL but also helps to understand the SM waveforms generated in a THz QCLs when they are used for various sensing and imaging applications.

Published by The Optical Society under the terms of the [Creative Commons Attribution 4.0 License](https://creativecommons.org/licenses/by/4.0/). Further distribution of this work must maintain attribution to the author(s) and the published article's title, journal citation, and DOI.

## 1. Introduction

Terahertz (THz) quantum cascade lasers (QCLs) are high-power sources of coherent radiation [1–4] in the THz band, a spectral region which has many unique properties, such as low photon energy, penetration of conventionally opaque materials, and provide spectral fingerprints for many biomolecules [5]. Laser feedback interferometry (LFI) is a coherent and self-detection technique where the emission source can be used as a highly-sensitive detector [6]. The combination of THz QCLs and LFI is particularly attractive and have been demonstrated in a wide variety of areas including chemical sensing, biomedical imaging, material analysis, and high-resolution spectroscopy [7].

In a typical LFI architecture, light emitted from the laser cavity is reflected from an external target. The reflected light imprinted with target information is reinjected into the laser cavity

where it interferes with the intra-cavity electric field and generates self-mixing (SM) signals. The time-varying SM signal is usually created by changing the length of the external cavity using a moving target or by laser frequency modulation through driving current sweeping for a static target [8]. The performance of an LFI sensor is highly dependent on the quality of the SM signals. For example, the fringe counting method is used to determine the target's displacement and in absolute distance measurements [9–13]; the time domain SM waveform can be used to extract the external cavity or target parameters [14]; and the Fourier transform of the SM signals were used to build amplitude and phase images of the target [15,16]. Therefore, physical effects that lead to abnormal variations in conventional SM waveforms may introduce errors in sensing and imaging measurements. For example, variation in laser emission modal structure can occur in the course of sensing or imaging, resulting in multiple peaks in each of the SM fringe, which has been observed in a variety of semiconductor lasers [17–20]. Correspondingly, signal processing algorithms have also been studied to compensate multi-mode induced SM multiplications [20,21]. In addition, fringe loss has been widely observed in a laser diode (LD) when it enters into the strong feedback regime [22–25]. It was demonstrated that the number of fringes is divided by 2 when  $7.8 < C < 14.0$  and by 3 when  $14.0 < C < 20.3$  [22] (The  $C$  parameter has been defined in Table 1). A clear explanation of the fringe loss phenomenon in an LD was provided in [25], which demonstrated that the significant tilts of SM fringes and the reduction of stable solutions for the excess phase equation for a given phase stimulus with boundaries due to either target movement or current sweeping resulted in fringe disappearance. However, to the best of our knowledge, fringe loss with increasing optical feedback (OF) strength in a THz QCL has not been reported so far.

In this work, we propose that the OF induced self-pulsations (SPs) — intrinsic OF dynamics — in THz QCLs, can lead to variations in conventional SM signal waveforms. We reported the first observation of SPs in a single-mode THz QCL under OF recently [26]. We demonstrated that the SPs observed originate from the beating between the lasing mode of the internal cavity and external cavity modes. This interaction results in periodic oscillations in emission power and terminal voltage of the THz QCL. Here in this work we provide a full demonstration of the SPs' effects on conventional SM fringes created by driving current sweeping and target movement

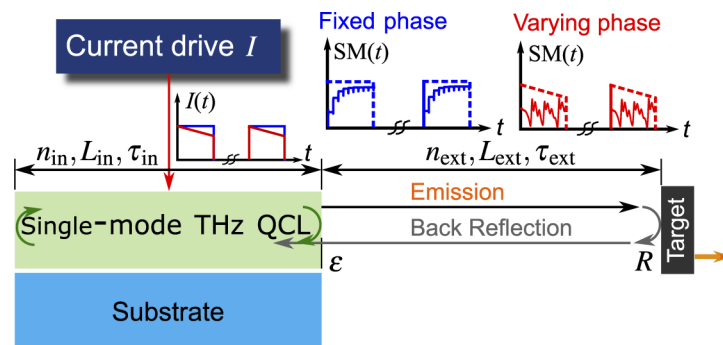


**Fig. 1.** The schematic system setup of a single-mode THz QCL under OF used for exploring SPs' effects on conventional SM signals created by driving current sweeping or target movement, where  $n_{in}$ ,  $L_{in}$ , and  $\tau_{in}$  are the refractive index, length, and round-trip time of the internal laser cavity, respectively. When the laser is driven by square pulses (the blue curves of  $I(t)$ ) and the target is static, namely, the reinjected optical field has a fixed phase, the SP phenomenon was observed (the blue curves in  $SM(t)$ ); while when the laser is driven by current sweeping (the red curves of  $I(t)$ ) or the target is moving, namely, the reinjected optical field has a varying phase, the SP dynamics are found superposed on SM interferometric fringes (the red curves in  $SM(t)$ ).

in a single-mode THz QCL system. In pulsed THz QCLs, when the duration of the pulse is on the same time scale as the period of the SPs (hundreds of nanoseconds), they appear as fine structure dynamics permanently modulating the emitted power waveform (see insets in Fig. 1). These SPs are further found superposed on conventional SM interferometric fringes when the reinjected optical field has a varying phase perturbation (resulting from driving current sweeping or target movement). Using a reduced rate equation (RRE) model, we separately explore the SM signal waveform under driving current sweeping and external target movement at varying OF strength *in silico*. The results of the modelling effort are experimentally validated using a pulsed-mode LFI system built around a THz QCL (see Fig. 1). The experimental waveform of the SM signal matches very well with the simulation results at varying OF strength. Additionally, the phenomenon of fringe loss in the SM signal — well known in LDs — is also observed along with pronounced SPs. All these variations to conventional SM waveforms may introduce errors in sensing measurements. Understanding the origin of SM waveform changes can help to understand the laser behaviour when they are used for various sensing and imaging applications.

The remainder of this article is organized as follows. Section 2 describes the theoretical model and experimental setup of the LFI system built around a THz QCL. The simulation and experimental results of the SM signal waveform from the THz QCL with driving current sweeping are shown in Section 3. The simulation results of the SM signal waveform with target movement with varying OF levels, or under external cavity lengths, or with varying pull back time of the target are shown in Supplement 1. Section 4 presents our conclusions.

## 2. Theoretical model and experimental setup

### 2.1. Theoretical model

We used single-mode RREs with OF terms as the theoretical model where the dependence of the input parameters on lattice temperatures and electric field (bias) are fully taken into account. Although the format of the RREs used here is similar to Ref. [27], the model that was used to calculate the RRE parameters at varying lattice temperatures and biases is different in this work. We used the density matrix (DM) model [28–36] instead of the full rate equation (RE) model in this work to obtain the RRE parameters at a range of lattice temperatures ( $T$ ) and biases ( $V$ ). The RRE input parameters include injection efficiencies  $\eta_3(T, V)$  and  $\eta_2(T, V)$ , electron transport parameters  $\tau_{sp}(T, V)$ ,  $\tau_3(T, V)$ ,  $\tau_{32}(T, V)$ ,  $\tau_{21}(T, V)$ , photon lifetime  $\tau_p(T, V)$  and gain factor  $G(T, V)$ . Compared with our published theoretical RREs model for single-mode THz QCL that used RE model [27,37,38], the DM model does not exhibit nonphysical spikes in the current density or material gain due to inclusion of coherent transport effects [34]. This theoretical model is an improved model of the well known Lang–Kobayashi model [39] which has been successfully applied to describe the dynamics of single-mode lasers under OF for the last three decades. By involving the voltage and temperature dependence of the input parameters, this set of RREs describes the interplay between electro-optical, thermal, and feedback effects which is the key to understanding the laser behaviour and SM waveforms.

A two-dimensional interpolation in  $T$  and  $V$  was then fitted to calculate values for each parameter at each time  $t$  with the lattice temperature  $T(t)$  calculated from Equation (5) and the bias  $V(t)$  corresponding to driving current  $I(t)$  and  $T(t)$  for use in Equations (1)–(4). The initial fitting process allows the RRE model to be solved for different choices of driving current excitation, ambient temperature, and OF strengths. The set of single-mode RREs read as follows:

$$\frac{dS(t)}{dt} = -\frac{1}{\tau_p(T, V)} S(t) + M \frac{\beta_{sp}}{\tau_{sp}(T, V)} N_3(t) + MG(T, V)(N_3(t) - N_2(t)) S(t) + \underbrace{\frac{2\kappa}{\tau_{in}} (S(t)S(t - \tau_{ext}(t)))^{\frac{1}{2}} \cos(\omega_{th}\tau_{ext} + \phi(t) - \phi(t - \tau_{ext}))}_{\text{Feedback Term}}, \quad (1)$$

$$\frac{d\phi(t)}{dt} = \frac{\alpha}{2} \left( MG(N_3(t) - N_2(t)) - \frac{1}{\tau_p(T, V)} \right) - \frac{\kappa}{\tau_{in}} \left( \frac{S(t - \tau_{ext}(t))}{S(t)} \right)^{\frac{1}{2}} \underbrace{\sin(\omega_{th} \tau_{ext} + \phi(t) - \phi(t - \tau_{ext}))}_{\text{Feedback Term}}, \quad (2)$$

$$\frac{dN_3(t)}{dt} = -G(T, V)(N_3(t) - N_2(t))S(t) - \frac{1}{\tau_3(T, V)}N_3(t) + \frac{\eta_3(T, V)}{q}I(t), \quad (3)$$

$$\frac{dN_2(t)}{dt} = +G(T, V)(N_3(t) - N_2(t))S(t) + \left( \frac{1}{\tau_{32}(T, V)} + \frac{1}{\tau_{sp}(T, V)} \right) N_3(t) - \frac{1}{\tau_{21}(T, V)}N_2(t) + \frac{\eta_2(T, V)}{q}I(t), \quad (4)$$

$$\frac{dT(t)}{dt} = \frac{1}{mc_p} \left( I(t)V(T(t), I(t)) - \frac{(T(t) - T_0(t))}{R_{th}} \right), \quad (5)$$

where  $N_3(t)$  and  $N_2(t)$  are the carrier populations in the upper and lower laser levels (ULL/LLL) of the active cavity, respectively, while  $S(t)$  and  $\phi(t)$  represent the photon population and the phase of the electric field. Once the equations are solved, the emission output power can be calculated by  $P_{out}(t) = \eta_0 \hbar \omega S(t) / \tau_p$ , where  $\eta_0 = \alpha_m / (2\alpha_{total})$  is power output coupling coefficient, where  $\alpha_m = \ln(R_2)^{-1} / L_{in}$  is the mirror loss of the laser cavity and  $\alpha_{total}$  is the total loss in the laser cavity, including the mirror loss and waveguide loss [40]. The meaning and value of other parameters are summarized in Table 1 if not described elsewhere.

## 2.2. Experimental setup

The system setup of the THz QCL under OF is shown in Fig. 1. The QCL consisted of a 12  $\mu\text{m}$ -thick AlGaAs/GaAs 9-well phonon-assisted active region [41]. Starting from the injection barrier, the layer sequence for each of the 95 periods is, **4/10.1/0.5/16.2/1/12.9/2/11.8/3/9.5/3/8.6/3/7.1/3/17/3/14.5 nm** (AlGaAs layers are shown in bold). The structure was grown by solid-source molecular beam epitaxy on a semi-insulating GaAs substrate, with the active region grown between doped upper 50 nm-thick ( $n = 5 \times 10^{18} \text{ cm}^{-3}$ ) and lower 700 nm thick ( $n = 2 \times 10^{18} \text{ cm}^{-3}$ ) GaAs contact layers. The wafer was processed into 150  $\mu\text{m}$  wide surface-plasmon ridge waveguide structures using photolithography and wet chemical etching, with the substrate thinned to 200  $\mu\text{m}$ . Devices were then mechanically cleaved to define a ridge of length 2 mm.

The laser was driven by a custom-built laser pulse driver that consisted of a main controller board with a field-programmable gate array (FPGA) controlling the pulse generation and SM signal extraction electronics. The driving current was set as ramping current pulse train starting from 0.97 A with a small linear current ramp about 120 mA, which is the driving current range that the laser has single-mode emission. The threshold current of the laser is around 0.8 A at 50 K. Each of the driving pulse is 450 ns long with duty cycle rate at 20%. The temperature of the laser was controlled by a compact cryogen-free Stirling cooler [16] and the operating point of the Stirling engine was set at 50 K. THz radiation from the THz QCL was collimated using a Tsurupica plastic lenses with 50 mm focal length and 30 mm clear aperture (Tsurupica-RR-CX-1.5-50-SPS, Broadband, Inc.). The target (a 2-inch gold mirror) was placed in the collimated path at varying distances from the QCL. A wire grid polarizer (G30-L, Microtech Instruments, Inc.) was used to vary the attenuation from 0 (100% transmission) to totally blocking the feedback beam (0% transmission). The SM signal was extracted from the voltage pulse measured across the laser by removing the leading and trailing edges of the pulse, subtracting a linear voltage ramp, and amplified as described in Ref. [16].

**Table 1. Parameters used in Eq. (1)–(5). Values for variables dependent on lattice temperature and voltage are given at  $T=50$  K and  $V=4.502$  V.**

Symbol	Description	Value / Units
$\eta_3(T, V)$	Injection efficiency into ULL	80.6 %
$\eta_2(T, V)$	Injection efficiency into LLL	0.18 %
$\tau_3(T, V)$	Total carrier lifetime in ULL	$10.84 \times 10^{-12}$ s
$\tau_{32}(T, V)$	Nonradiative relaxation time from ULL to LLL	$6.18 \times 10^{-9}$ s
$\tau_2(T, V)$	Total carrier lifetime in LLL	$3.63 \times 10^{-13}$ s
$\tau_{sp}(T, V)$	Spontaneous emission lifetime	$2.83 \times 10^{-5}$ s
$\tau_p(T, V)$	Photon lifetime	$2.29 \times 10^{-12}$ s
$G(T, V)$	Gain factor	$1.13 \times 10^4$ s <sup>-1</sup>
$M$	Number of periods in active cavity	95
$\beta_{sp}$	Spontaneous emission factor	$1.627 \times 10^{-4}$
$\omega_{th}$	Emission frequency with no OF	$2\pi \times 2.80$ THz
$L_{ext}$	Initial external cavity length	1.6 m
$n_{ext}$	Refractive index of external cavity	1.00
$\tau_{ext}$	Round-trip time of the external laser cavity, $\tau_{ext} = 2L_{ext}n_{ext}/c$	$1.067 \times 10^{-8}$ s
$L_{in}$	Laser cavity length	2 mm
$n_{in}$	Refractive index of active region	3.3
$\tau_{in}$	Round-trip time of internal laser cavity, $\tau_{in} = 2L_{in}n_{in}/c$	$4.403 \times 10^{-11}$ s
$\kappa$	Feedback coupling coefficient, $\kappa = \varepsilon\sqrt{R/R_2}(1 - R_2)$	Varies
$\tilde{\kappa}$	Feedback coupling rate, $\tilde{\kappa} = \kappa/\tau_{in}$	Varies
$\varepsilon$	Re-injection coupling factor	Varies
$R$	Reflectivity of external target	0.7
$R_2$	Internal reflection coefficient of emitting laser facet	0.2861
$\alpha$	Linewidth enhancement factor	-0.1
$C$	Feedback parameter, $C = \tilde{\kappa}\tau_{ext}\sqrt{1 + \alpha^2}$	Varies
$m$	Effective mass of laser chip	$1.91 \times 10^{-8}$ kg
$c_p$	Effective specific heat capacity of laser chip	$330$ J kg <sup>-1</sup> K <sup>-1</sup>
$R_{th}$	Effective thermal resistance – laser chip to cold finger	$5$ K W <sup>-1</sup>
$T_0$	Cold finger temperature	50 K
$q$	Elementary charge	$1.602 \times 10^{-19}$ C
$c$	Speed of light in vacuum	$299792458$ m s <sup>-1</sup>
$f_{EC}$	External cavity resonant frequency $f_{EC} = c/(2n_{ext}L_{ext})$	93.69 MHz

### 3. Simulation and experiment results

There are two convenient ways to create SM interferometric signals: sweeping the driving current (thereby varying the emission frequency) and target movement (thereby varying the external cavity length) [8]. The results with driving current sweeping and a static target are demonstrated in this section, while those with a moving target and constant driving current are presented in [Supplement 1](#).

The emission power from the THz QCL under OF ( $P_{out}(t)$ ) with the parameters shown in Table 1 was simulated with current sweeping linearly from 0.97 A down by 120 mA within 200 ns, and a cold finger temperature  $T_0$  set at 50 K. We emulate a linear frequency sweep with the driving current to be 12 MHz/mA [27]. The reference of the emission power ( $P_0(t)$ ) was

calculated by solving RREs without OF (setting  $\varepsilon=0$ ). The SM signal, namely,  $P_{\text{out}}(t) - P_0(t)$ , is plotted in Fig. 2 with increasing feedback strengths of  $\varepsilon$  from  $-60$  dB to  $0$  dB. The SM waveform from the THz QCL undergoes four different regimes when the OF increases from very weak feedback to strongest feedback. They are Regime 1: regular SM interferometric fringes at  $\varepsilon = -60$  dB and  $C = 0.27$  (Fig. 2(a)); Regime 2: SPs modulated on full SM fringes around  $f_{\text{EC}}$  when  $\varepsilon$  is  $-40$  dB and  $C$  is  $2.72$  (Fig. 2(b)). Due to the fact that the self-interference was renewed after each fringe traverses a peak and trough of one interference period, the modulation of the SPs on each of the SM fringe was also renewed. Passing through the fringe is equivalent to changing the reflectivity of the target or the equivalent of changing the position on the light current curve (essentially acting as a small current pulse); Regime 3: SPs modulated on reduced number of SM fringes (fringe loss) around the external cavity resonant frequency  $f_{\text{EC}}$  as defined in Table 1 when  $\varepsilon$  is varied from  $-30$  dB to  $-20$  dB with  $C$  increasing from  $8.60$  to  $27.21$ , the number of SM fringes reduced to 3, 2, and 1 in Fig. 2(c), (d), and (e), respectively; and ultimately Regime 4: all SM fringes disappear and only SPs with decreasing amplitude remaining under the strongest feedback strength at  $\varepsilon = 0$  dB and  $C = 272.06$  in Fig. 2(f). Fringe loss is a well-known phenomenon in LDs under OF as a consequence of the jumps of solutions of the excess phase equation under strong feedback. However, fringe loss in THz QCLs under OF has not been reported so far. In addition, the modulation of the SPs on the full or lost SM fringes was not observed in LDs due to more complex laser dynamics (coherence collapse) dominant in LDs [42].

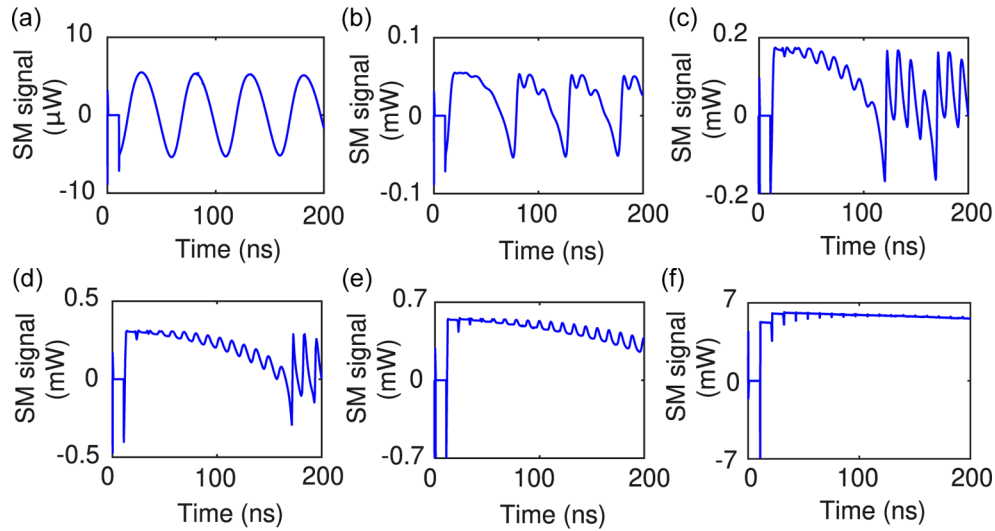


**Fig. 2.** Simulated SM signal for the THz QCL under feedback with current sweeping for 120 mA where  $L_{\text{ext}}=1.6$  m, with increasing feedback strength from (a)  $\varepsilon = -60$  dB,  $C = 0.27$ ; (b)  $\varepsilon = -40$  dB,  $C = 2.72$ ; (c)  $\varepsilon = -30$  dB,  $C = 8.60$ ; (d)  $\varepsilon = -25$  dB,  $C = 15.29$ ; (e)  $\varepsilon = -20$  dB,  $C = 27.21$ ; (f)  $\varepsilon = 0$  dB,  $C = 272.06$ .

The experimental setup as described in Fig. 1 was used to validate the simulated SPs in a THz QCL with driving current sweeping and under OF from a static target. Figure 3 depicts the measured SM signal (red curves) at various OF strengths when the polarizer was tuned to vary the attenuation in the external cavity. As a comparison, the simulated SM signal with varying feedback parameter  $C$  is scaled and plotted as well (blue curves). As a reference, the result with no OF is shown in Fig. 3(a) with the reflected beam from the mirror totally blocked by a envelope with a metallic film. Due to the rise-time of the driving current pulse and the gating circuit from the SM signal extraction electronics, the initial segment of data (covered by the gray box) was



not included in the red experimental curves. Regular fringes are observed at weak feedback as shown in Fig. 3(b), which agrees well with the simulated result when  $\varepsilon = -60$  dB and  $C = 0.27$ . SPs which appear as periodic oscillations at each of the fringes start in Fig. 3(c), where the SM waveform also agrees with the simulated result with  $\varepsilon = -42.67$  dB and  $C = 2.00$ . When the OF is further increased, the periodic oscillation amplitude is enhanced in Fig. 3(d), where the SM waveform follow the similar profile with the simulated result with  $\varepsilon = -37.81$  dB and  $C = 3.50$ . Due to the nonlinear emission frequency changes with the driving current in the THz QCL, the number of oscillation periods or ripples on each of the fringes are not identical. Periodic

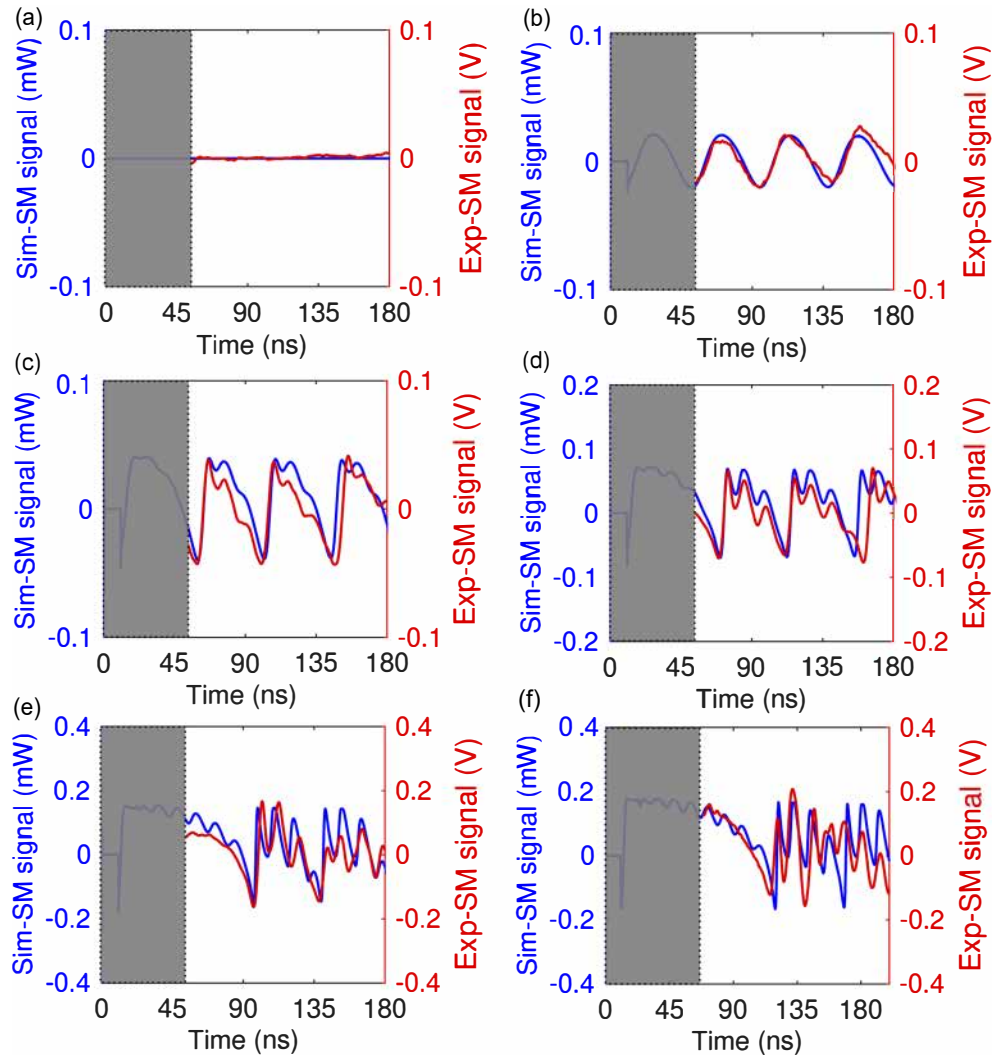


**Fig. 3.** Comparison between simulated (blue curves) SM signal and experimental (red curves) SM signal from the THz QCL under varying OF strength with the attenuation in the external cavity tuned by the polarizer: (a) no OF; (b) regular SM fringes when  $\varepsilon = -60$  dB and  $C = 0.27$ ; (c) full fringes with oscillations when  $\varepsilon = -42.67$  dB and  $C = 2.00$ ; (d) fringe loss with oscillations when  $\varepsilon = -37.81$  dB and  $C = 3.50$ ; (e) fringe loss with oscillations when  $\varepsilon = -31.19$  dB and  $C = 7.50$ ; (f) fringe loss with oscillations when  $\varepsilon = -30$  dB and  $C = 8.60$ .

oscillations superposed on reduced number of fringes is observed in Fig. 3(e) with stronger OF, which qualitatively agrees with the simulated result when  $\varepsilon = -31.19$  dB and  $C = 7.50$ . Periodic oscillations around  $f_{EC}$  with further reduced number of fringes were observed experimentally in Fig. 3(f) when the polarizer was set at 100% transmission, which is close to the simulation result with  $\varepsilon = -30$  dB and  $C = 8.60$ . This is the strongest achievable OF experimentally. However, the laser dynamics of the SPs superposed on full SM fringes and fringe loss were successfully captured in the experiment. It was also observed that the first dip in the SM signal shifts to longer times, which is a manifestation of the fringe loss and was observed in both simulation and experiment. As feedback increased the fringes are stretched out and lost and thus the initial delay increases. In addition, the SP oscillation frequency increases with the OF level as demonstrated in [26,43]. The SP oscillation frequency of the simulation results in Fig. 3(c), (d),(e),(f) are 70 MHz, 72.5 MHz, 90 MHz, and 92.5 MHz, respectively. The SM frequency is around 20 MHz before fringe loss dominants in Fig. 3(c), (d).

The abnormal waveforms of SM signals induced by SP modulation may introduce errors when THz QCLs are used in sensing and imaging applications, therefore has to be considered and compensated for during the signal processing process. For the THz sensing and imaging applications based on SM, the SP modulations can be observed when the  $C$  parameter is around and larger than 2. However, the SP phenomenon itself can also be used for THz sensing and imaging since the SP amplitude and the oscillation frequency is a monotonic function of the optical feedback level [43]. The optical feedback dynamics associated with SPs and the modulation on SM signals are highly dependent on the linewidth enhancement factor. However, modulation properties demonstrated in this work would not change qualitatively as long as the value of the linewidth enhancement factor is within the range for THz QCLs, which is typically less than 1 [44,45], as recently measured [46,47].

#### 4. Conclusion

In conclusion, we investigated the influences of the intrinsic SP dynamics from a THz QCL under OF on the conventional SM signal created by driving current sweeping and target movement. It is found the SP dynamics modulated on SM interferometric fringes at varying OF levels. Moreover, we observed fringe loss in THz QCLs under strong feedback conditions, which is the first report of fringe loss in THz QCLs, to the best of our knowledge.

The variations of the SM waveform created by driving current sweeping under increasing OF strengths are demonstrated theoretically and experimentally, which matches with each other very well at varying OF strength. This SM waveform transition route with increasing OF strengths was also identified when the THz QCL was under OF from a moving target (with constant driving current). Furthermore, it was found that the changes of the SM waveform from the optically reinjected THz QCL also depends on the ratio of the external round trip time over target pullback time. For a fixed OF strength, the higher the ratio, the larger the number of ripples or oscillation periods was found on each fringe. In addition, when the external cavity length varies while other parameters remain unchanged, the SM waveform experiences a combination effects consisting of the SPs with a varying fundamental frequency and fringe loss due to increasing feedback parameter  $C$ . These variations of the SM signal waveform induced by SPs need to be considered when THz QCLs are used for sensing and imaging applications.

**Funding.** Advance Queensland Industry Research Fellowships; Engineering and Physical Sciences Research Council (EP/J002356/1, EP/P021859/1, EP/T034246/1); Australian Research Council (DP20010194).

**Disclosures.** The authors declare no conflicts of interest.

**Data availability.** Data underlying the results presented in this paper are not publicly available at this time but may be obtained from the authors upon reasonable request.

**Supplemental document.** See [Supplement 1](#) for supporting content.



## References

1. R. Köhler, A. Tredicucci, F. Beltram, H. E. Beere, E. H. Linfield, A. G. Davies, D. A. Ritchie, R. C. Iotti, and F. Rossi, "Terahertz semiconductor-heterostructure laser," *Nature* **417**(6885), 156–159 (2002).
2. B. S. Williams, S. Kumar, Q. Hu, and J. L. Reno, "High-power terahertz quantum cascade lasers," in *2006 Conference on Lasers and Electro-Optics and 2006 Quantum Electronics and Laser Science Conference*, (Long Beach, United States, 2006), pp. 1–2.
3. L. H. Li, L. Chen, J. Freeman, M. Salih, P. Dean, A. G. Davies, and E. H. Linfield, "Multi-watt high-power THz frequency quantum cascade lasers," *Electron. Lett.* **53**(12), 799–800 (2017).
4. A. Khalatpour, A. K. Paulsen, C. Deimert, Z. R. Wasilewski, and Q. Hu, "High-power portable terahertz laser systems," *Nat. Photonics* **15**(1), 16–20 (2021).
5. M. Tonouchi, "Cutting-edge terahertz technology," *Nat. Photonics* **1**(2), 97–105 (2007).
6. T. Taimre, M. Nikolić, K. Bertling, Y. L. Lim, T. Bosch, and A. D. Rakić, "Laser feedback interferometry: a tutorial on the self-mixing effect for coherent sensing," *Adv. Opt. Photonics* **7**(3), 570–631 (2015).
7. A. D. Rakić, T. Taimre, K. Bertling, Y. L. Lim, P. Dean, A. Valavanis, and D. Indjin, "Sensing and imaging using laser feedback interferometry with quantum cascade lasers," *Appl. Phys. Rev.* **6**(2), 021320 (2019).
8. A. D. Rakić, T. Taimre, K. Bertling, Y. L. Lim, P. Dean, D. Indjin, Z. Ikonić, P. Harrison, A. Valavanis, S. P. Khanna, M. Lachab, S. J. Wilson, E. H. Linfield, and A. G. Davies, "Swept-frequency feedback interferometry using terahertz frequency QCLs: a method for imaging and materials analysis," *Opt. Express* **21**(19), 22194–22205 (2013).
9. M. Norgia and S. Donati, "A displacement-measuring instrument utilizing self-mixing interferometry," *IEEE Trans. Instrum. Meas.* **52**(6), 1765–1770 (2003).
10. A. Tarun, J. Jecong, and C. Saloma, "In-line interferometer for direction-sensitive displacement measurements by optical feedback detection," *Appl. Opt.* **44**(34), 7287–7294 (2005).
11. Y. L. Lim, P. Dean, M. Nikolić, R. Kliese, S. P. Khanna, M. Lachab, A. Valavanis, D. Indjin, Z. Ikonić, P. Harrison, E. H. Linfield, A. G. Davies, S. J. Wilson, and A. D. Rakić, "Demonstration of a self-mixing displacement sensor based on terahertz quantum cascade lasers," *Appl. Phys. Lett.* **99**(8), 081108 (2011).
12. F. Mezzapesa, L. Columbo, M. Dabbicco, M. Brambilla, and G. Scamarcio, "QCL-based nonlinear sensing of independent targets dynamics," *Opt. Express* **22**(5), 5867–5874 (2014).
13. E. Gagnon and J.-F. Rivest, "Laser range imaging using the self-mixing effect in a laser diode," *IEEE Trans. Instrum. Meas.* **48**(3), 693–699 (1999).
14. S. Han, K. Bertling, P. Dean, J. Keeley, A. D. Burnett, Y. L. Lim, S. P. Khanna, A. Valavanis, E. H. Linfield, A. G. Davies, D. Indjin, T. Taimre, and A. D. Rakić, "Laser feedback interferometry as a tool for analysis of granular materials at terahertz frequencies: Towards imaging and identification of plastic explosives," *Sensors* **16**(3), 352 (2016).
15. Y. L. Lim, T. Taimre, K. Bertling, P. Dean, D. Indjin, A. Valavanis, S. P. Khanna, M. Lachab, H. Schaidler, T. W. Prow, H. P. Soyer, S. J. Wilson, E. H. Linfield, A. G. Davies, and A. D. Rakić, "High-contrast coherent terahertz imaging of porcine tissue via swept-frequency feedback interferometry," *Biomed. Opt. Express* **5**(11), 3981–3989 (2014).
16. Y. L. Lim, K. Bertling, T. Taimre, T. Gillespie, C. Glenn, A. Robinson, D. Indjin, Y. Han, L. Li, E. H. Linfield, A. G. Davies, P. Dean, and A. D. Rakić, "Coherent imaging using laser feedback interferometry with pulsed-mode terahertz quantum cascade lasers," *Opt. Express* **27**(7), 10221–10233 (2019).
17. J. R. Tucker, A. D. Rakić, C. J. O'Brien, and A. V. Zvyagin, "Effect of multiple transverse modes in self-mixing sensors based on vertical-cavity surface-emitting lasers," *Appl. Opt.* **46**(4), 611–619 (2007).
18. M. Ruiz-Llata and H. Lamela, "Self-mixing technique for vibration measurements in a laser diode with multiple modes created by optical feedback," *Appl. Opt.* **48**(15), 2915–2923 (2009).
19. J. Keeley, J. Freeman, K. Bertling, Y. L. Lim, R. A. Mohandas, T. Taimre, L. H. Li, D. Indjin, A. D. Rakić, E. H. Linfield, A. G. Davies, and P. Dean, "Measurement of the emission spectrum of a semiconductor laser using laser-feedback interferometry," *Sci. Rep.* **7**(1), 7236 (2017).
20. U. Zabit, K. Shaheen, M. Naveed, O. D. Bernal, and T. Bosch, "Automatic detection of multi-modality in self-mixing interferometer," *IEEE Sens. J.* **18**(22), 9195–9202 (2018).
21. M. Usman, U. Zabit, O. D. Bernal, G. Raja, and T. Bosch, "Detection of multimodal fringes for self-mixing-based vibration measurement," *IEEE Trans. Instrum. Meas.* **69**(1), 258–267 (2020).
22. Y. Yu, J. Xi, J. F. Chicharo, and T. M. Bosch, "Optical feedback self-mixing interferometry with a large feedback factor C: Behavior studies," *IEEE J. Quantum Electron.* **45**(7), 840–848 (2009).
23. R. Kliese, T. Taimre, A. A. Bakar, Y. L. Lim, K. Bertling, M. Nikolić, J. Perchoux, T. Bosch, and A. D. Rakić, "Solving self-mixing equations for arbitrary feedback levels: a concise algorithm," *Appl. Opt.* **53**(17), 3723–3736 (2014).
24. O. D. Bernal, U. Zabit, and T. Bosch, "Classification of laser self-mixing interferometric signal under moderate feedback," *Appl. Opt.* **53**(4), 702–708 (2014).
25. M. Veng, J. Perchoux, and F. Bony, "Fringe disappearance in self-mixing interferometry laser sensors: Model and application to the absolute distance measurement scheme," *IEEE Sens. J.* **19**(14), 5521–5528 (2019).
26. X. Qi, K. Bertling, T. Taimre, G. Agnew, Y. L. Lim, T. Gillespie, A. Robinson, M. Brúnig, A. Demić, P. Dean, L. H. Li, E. H. Linfield, A. G. Davies, D. Indjin, and A. D. Rakić, "Observation of optical feedback dynamics in single-mode terahertz quantum cascade lasers: Transient instabilities," *Phys. Rev. A* **103**(3), 033504 (2021).

27. G. Agnew, A. Grier, T. Taimre, Y. L. Lim, K. Bertling, Z. Ikonić, A. Valavanis, P. Dean, J. Cooper, S. P. Khanna, M. Lachab, E. H. Linfield, A. G. Davies, P. Harrison, D. Indjin, and A. D. Rakić, "Model for a pulsed terahertz quantum cascade laser under optical feedback," *Opt. Express* **24**(18), 20554–20570 (2016).
28. H. Callebaut and Q. Hu, "Importance of coherence for electron transport in terahertz quantum cascade lasers," *J. Appl. Phys.* **98**(10), 104505 (2005).
29. K. Blum, *Density matrix theory and applications*, vol. 64 (Springer Science & Business Media, 2012).
30. E. Dupont, S. Fatholouloumi, and H. Liu, "Simplified density-matrix model applied to three-well terahertz quantum cascade lasers," *Phys. Rev. B* **81**(20), 205311 (2010).
31. B. A. Burnett and B. S. Williams, "Density matrix model for polarons in a terahertz quantum dot cascade laser," *Phys. Rev. B* **90**(15), 155309 (2014).
32. O. Jonasson, F. Karimi, and I. Knezevic, "Partially coherent electron transport in terahertz quantum cascade lasers based on a markovian master equation for the density matrix," *J. Comput. Electron.* **15**(4), 1192–1205 (2016).
33. A. Pan, B. A. Burnett, C. O. Chui, and B. S. Williams, "Density matrix modeling of quantum cascade lasers without an artificially localized basis: A generalized scattering approach," *Phys. Rev. B* **96**(8), 085308 (2017).
34. A. Demić, A. Grier, Z. Ikonić, A. Valavanis, C. A. Evans, R. Mohandas, L. Li, E. H. Linfield, A. G. Davies, and D. Indjin, "Infinite-period density-matrix model for terahertz-frequency quantum cascade lasers," *IEEE Trans. Terahertz Sci. Technol.* **7**(4), 368–377 (2017).
35. B. A. Burnett, A. Pan, C. O. Chui, and B. S. Williams, "Robust density matrix simulation of terahertz quantum cascade lasers," *IEEE Trans. Terahertz Sci. Technol.* **8**(5), 492–501 (2018).
36. A. Demić, Z. Ikonić, R. W. Kelsall, and D. Indjin, "Density matrix superoperator for periodic quantum systems and its application to quantum cascade laser structures," *AIP Adv.* **9**(9), 095019 (2019).
37. G. Agnew, A. Grier, T. Taimre, Y. L. Lim, M. Nikolić, A. Valavanis, J. Cooper, P. Dean, S. P. Khanna, M. Lachab, E. H. Linfield, A. G. Davies, P. Harrison, Z. Ikonić, D. Indjin, and A. D. Rakić, "Efficient prediction of terahertz quantum cascade laser dynamics from steady-state simulations," *Appl. Phys. Lett.* **106**(16), 161105 (2015).
38. G. Agnew, A. Grier, T. Taimre, K. Bertling, Y. L. Lim, Z. Ikonić, P. Dean, A. Valavanis, D. Indjin, and A. D. Rakić, "Frequency tuning range control in pulsed terahertz quantum-cascade lasers: Applications in interferometry," *IEEE J. Quantum Electron.* **54**(2), 1–8 (2018).
39. R. Lang and K. Kobayashi, "External optical feedback effects on semiconductor injection laser properties," *IEEE J. Quantum Electron.* **16**(3), 347–355 (1980).
40. L. A. Coldren, S. W. Corzine, and M. L. Mashanovitch, *Diode lasers and photonic integrated circuits* (John Wiley & Sons, 2012).
41. M. Wienold, L. Schrottke, M. Giehler, R. Hey, W. Anders, and H. Grahn, "Low-voltage terahertz quantum-cascade lasers based on lo-phonon-assisted interminiband transitions," *Electron. Lett.* **45**(20), 1030–1031 (2009).
42. G. Giuliani and S. Donati, *Unlocking Dynamical Diversity: Optical Feedback Effects on Semiconductor lasers*, (Wiley, 2005).
43. X. Qi, K. Bertling, T. Taimre, Y. L. Lim, T. Gillespie, P. Dean, L. H. Li, E. H. Linfield, A. G. Davies, D. Indjin, and A. D. Rakić, "Terahertz imaging with self-pulsations in quantum cascade lasers under optical feedback," *APL Photonics* **6**(9), 091301 (2021).
44. M. Yamanishi, T. Edamura, K. Fujita, N. Akikusa, and H. Kan, "Theory of the intrinsic linewidth of quantum-cascade lasers: Hidden reason for the narrow linewidth and line-broadening by thermal photons," *IEEE J. Quantum Electron.* **44**(1), 12–29 (2008).
45. F. P. Mezzapesa, L. L. Columbo, M. Brambilla, M. Dabbicco, S. Borri, M. S. Vitiello, H. E. Beere, D. A. Ritchie, and G. Scamarcio, "Intrinsic stability of quantum cascade lasers against optical feedback," *Opt. Express* **21**(11), 13748–13757 (2013).
46. R. P. Green, J.-H. Xu, L. Mahler, A. Tredicucci, F. Beltram, G. Giuliani, H. E. Beere, and D. A. Ritchie, "Linewidth enhancement factor of terahertz quantum cascade lasers," *Appl. Phys. Lett.* **92**(7), 071106 (2008).
47. M. S. Vitiello, L. Consolino, S. Bartalini, A. Taschin, A. Tredicucci, M. Inguscio, and P. De Natale, "Quantum-limited frequency fluctuations in a terahertz laser," *Nat. Photonics* **6**(8), 525–528 (2012).